PERGAMON

Journal of Structural Geology 22 (2000) 1761–1771

JOURNAL OF STRUCTURAL GEOLOGY

www.elsevier.nl/locate/jstrugeo

# Anisotropy of diamagnetic susceptibility in Thassos marble: A comparison between measured and modeled data

Helga de Wall[a,*], Michel Bestmann[b], Klaus Ullemeyer[c]

[a]*Geologisch-Paläontologisches Institut, Ruprecht-Karls-Universität, Im Neuenheimer Feld 234, D-69120 Heidelberg, Germany*
[b]*Institut für Geologie und Mineralogie, Schlossgarten 5, D-91054 Erlangen, Germany*
[c]*Institut für Geologie und Dynamik der Lithosphäre, Goldschmidtstr. 3, D-37077 Göttingen, Germany*

Received 3 December 1999; accepted 27 June 2000

**Abstract**

A study of shear zones within the calcite marble complex of the island of Thassos (Greece) shows that the low field anisotropy of magnetic susceptibility (AMS)-technique can be successfully applied to diamagnetic rocks for characterizing rock fabrics. The strain path involves both an early pure shear stage and a simple shear overprint that is documented by a transition from triaxial (neutral) to uniaxial (prolate) shapes of AMS ellipsoids. The maximum susceptibility is oriented perpendicular to the rock foliation, reflecting the preferred orientation of calcite *c*-axes in the protolith as well as in the mylonites. For three samples that represent different types of calcite fabrics, the AMS was recalculated from neutron and electron backscatter diffraction textural data. A comparison of the measured and modeled data shows a good coincidence for the orientation of the principal AMS axes and for the recalculated anisotropy data. Both measured and modeled data sets reflect the change from neutral to distinct prolate ellipsoids during progressive deformation. © 2000 Elsevier Science Ltd. All rights reserved.

## 1. Introduction

Besides quartz and feldspar, calcite is the most important rock forming mineral that shows diamagnetic behavior. Due to its crystal structure, calcite has a uniaxial magnetic anisotropy with a maximum value parallel to the *c*-axis. The degree of anisotropy, *P* (maximum divided by minimum susceptibility) for calcite is 1.113 (Owens and Bamford, 1976), which is significantly higher than for quartz with 1.01, and lower than for orthoclase with 1.23 (Borradaile, 1987). In the work of Rutter and Rusbridge (1977) and Owens and Rutter (1978), significant anisotropies were recorded from high field susceptibility measurements (1 T field) conducted on experimentally deformed Carrara marble that showed AMS-ellipsoids with prolate geometries ($k_{max} >> k_{int} = k_{min}$).

Although it has been demonstrated experimentally that the fabric parameters of carbonate rocks determined by measurements of the anisotropy of magnetic susceptibility (AMS) are consistent with results from optical fabric studies (Owens and Rutter, 1978), the implications of this work have not been applied to natural field studies. This probably reflects the rarity of natural calcite rocks that show a pure diamagnetic behavior, where interference from paramagnetic minerals can be excluded. The presence of even minor paramagnetic contributions in the rocks mineralogy can cause interference between dia- and paramagnetic subfabrics, leading to unrealistically high anisotropy values that are not suitable for fabric interpretations (Hrouda, 1986).

This paper presents a study of the marble complex from the island of Thassos, Greece that shows pure diamagnetic behavior of susceptibility in low magnetic fields. The so-called Thassos-marble is a well-known ornamental rock famous because of its massive equigranular habit and its pale white color. It consists of nearly 100% calcite, with only rare quartz and dolomite grains (Bestmann et al., 2000). It forms part of the metamorphic succession of Thassos, which shows fabric development under retrograde metamorphic conditions that can be linked to the exhumation of the Rhodope metamorphic core complex (Peterek et al., 1994; Wawrzenitz and Krohe, 1998, Fig. 1). During the exhumation, strain localization occurred at decreasing pressure–temperature conditions. Several shear zones of up to 3 m in thickness in the marble complexes can be related to this stage of deformation. The microstructural and textural fabrics and their kinematic significance are dealt with in Bestmann et al. (2000).

* Corresponding author. Fax: +49-6221-545503.
*E-mail address:* hr8@ix.urz.uni-heidelberg.de (H. de Wall).

0191-8141/00/$ - see front matter © 2000 Elsevier Science Ltd. All rights reserved.
PII: S0191-8141(00)00105-X

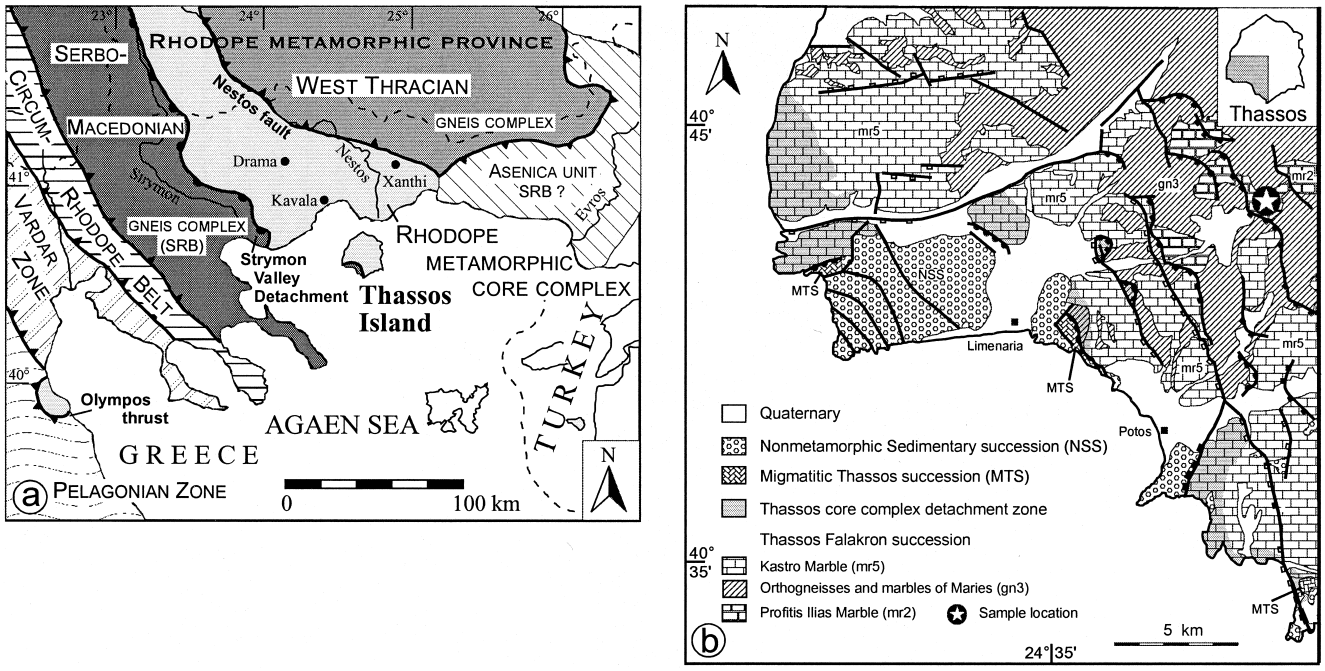


Fig. 1. Tectonometamorphic units in the north Aegean region (NE Greece) (a) and sample location on the island of Thassos (b).

In our study we have investigated a 4.5 m thick section in the Kastro valley across shear zones within the marble complex (Fig. 2). It has been analyzed whether a correlation between AMS and calcite texture is valid, and whether the AMS-technique can be applied to characterize naturally deformed calcite rocks.

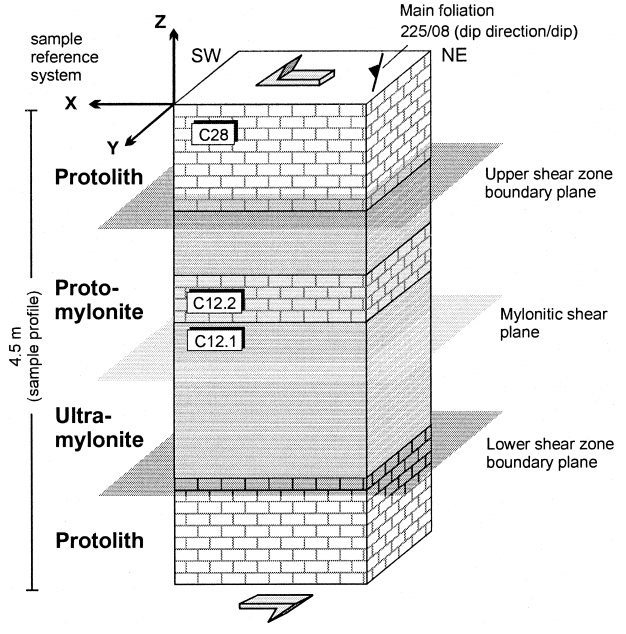


Fig. 2. Sketch of the Thassos marble shear zone complex and location of specimens for the comparison of magnetic fabric and calcite texture. Sample reference system (*X*, *Y*, *Z*) and bulk shear sense (sinistral) are given.

### *1.1. Sample characterization*

The massive marble (protolith) shows decimeter to meter thick bedding. Faint color banding (grey–blue and white) defines a macroscopic main foliation that dips gently towards the SW (225/08). The shear zone complex is characterized by a sharp fabric transition from the coarse-grained protolith to the homogeneous, extremely fine-grained ultramylonite, which locally shows a laminated fabric. This mylonitic foliation also dips gently towards the SW and is parallel to the shear zone boundary. Therefore all main tectonic planes of the Thassos marble shear zone complex are observed to be subparallel. The shear zone boundary surface (SZB), in combination with the shear direction (*X*), is used as a reference system for the presentation of the calcite textures and the AMS tensors.

The massive marble is equigranular and coarse-grained (grain size 1–3 mm) with high twin-lamellae density (Fig. 3a). Traces of two equally developed sets of twins are oriented both clockwise and anticlockwise with respect to the long axes that are approximately aligned within the mesoscopic foliation. The transition into the shear zone is marked by a sharp reduction in grain size, with a narrow zone of protomylonitic fabric, characterized by inhomogeneous microfabrics. Within the protomylonitic fabric domains, the grain long axes and a dominant twin system in the porphyroclasts are oriented oblique to the SZB (Fig. 3b). The fine-grained ultramylonite in the interior of the shear zone is pervasively recrystallized with a generally homogeneous microstructure (Fig. 3c). The deformation is characteristically dominated by dynamic recrystallization

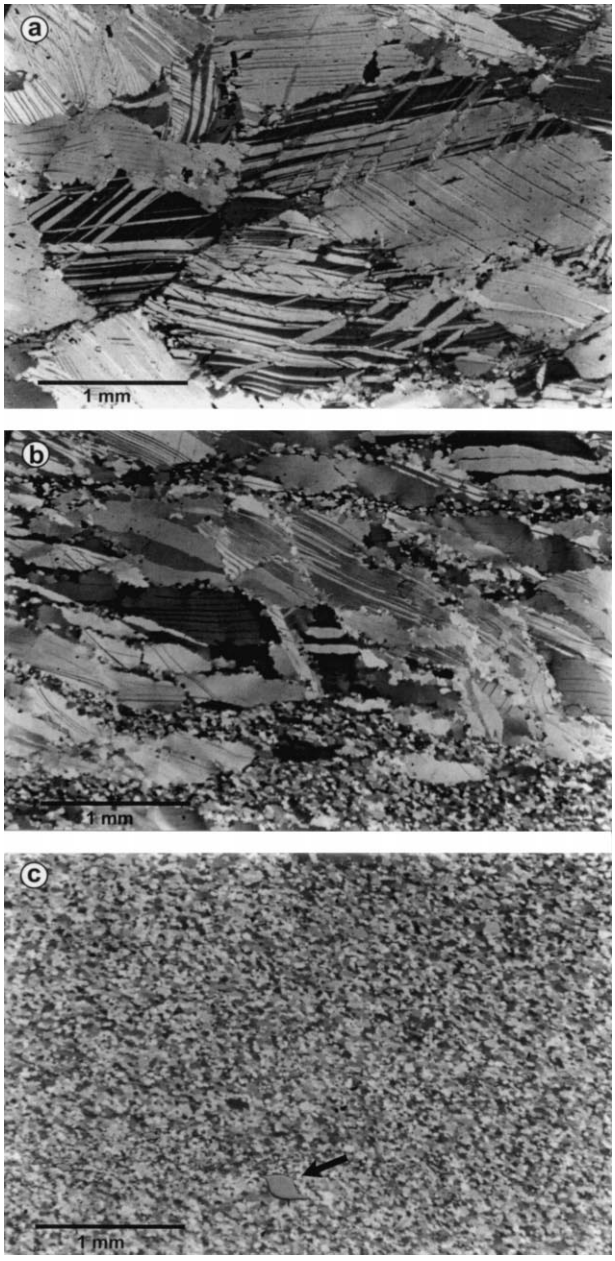


Fig. 3. Photomicrographs from the three types of calcite fabric taken in reflected polarized light from high-polished slab (*XZ*-sections). (a) Protolith with different sets of twins (sample C28); (b) Transition from protomylonite to mylonite (sample C12.2); (c) Ultramylonite, the arrow marks a σ-shaped quartz grain, indicating simple shear deformation (sample C12.1).

accompanied by a strong grain size reduction (grain size 10–30 μm). These recrystallized grains are generally free of twins. Mylonitization under dominantly non-coaxial deformation conditions within the shear zone is indicated by a grain shape preferred orientation lying oblique to the SZB. The asymmetric shape of quartz grains incorporated in the calcite matrix gives further evidence for dominant simple shear during strain localization within the shear zone (Bestmann et al., 2000).

## 2. Texture analyses

Three samples representing characteristic examples for the different fabric domains (protolith, protomylonite, ultramylonite) have been selected for detailed comparison of the texture and magnetic fabric. The position of the samples in the shear zone complex is shown in Fig. 2. For these three samples the preferred crystallographic orientation was measured and this textural data subsequently used to recalculate the AMS.

For the coarse-grained protolith and protomylonites, calcite textures were determined by the neutron diffraction technique. The measurements were performed using the time-of-flight (TOF) texture diffractometer at the Frank Laboratory of Neutron Physics, Dubna (Russia), which has been especially designed for fast texture measurements (Ullemeyer et al., 1998). Neutrons offer the advantage of low absorption in matter, hence more coarse-grained samples can be investigated than by using X-rays. Furthermore, the same samples used for the AMS measurements could be analyzed in the neutron experiment, with the obvious advantage that both data sets are determined by averaging from the same portion of rock. Six pole figures (01-12, 10-14, 0001, 11-20, 11-23 and 01-18 + 02-14) were extracted from the TOF patterns and used as input to calculate the orientation distribution function (ODF) applying the WIMV algorithm as implemented in the BEARTEX program package (Matthies and Vinel, 1982; Wenk et al., 1998). From the ODF, the pole figures useful for kinematic interpretations were recalculated.

The texture of the fine-grained ultramylonite was determined from electron backscatter diffraction (EBSD) patterns (Adams et al., 1994; Kunze et al., 1994). The experimental set up is described by Van Daalen et al. (1999). The individual orientation data were processed by Gaussian convolution with a smoothing width of 15° using the harmonic calculus. From the resulting ODF, pole figures were calculated and presented for a representative sample (C12.1) in a comparable way to those of the coarse-grained samples (C28, C12.2) obtained from neutron diffraction. The *c*-axis pole figures of the three samples are discussed in the following section (refer to Bestmann et al. (2000) for the complete texture information).

The texture of the protolith (C28) is characterized by a single *c*-axis maximum oriented perpendicular to the SZB (Fig. 4). However, a weak girdle tendency around an axis that deviates from the *X*-direction is evident. Neglecting the asymmetric relationship to the external reference frame, such textures are comparable with the patterns of experimentally deformed calcite marbles and simulated textures under pure shear conditions in the twinning regime (e.g. Wenk et al., 1987). The overall microfabric (texture and microstructure) of the protolith shows a nearly orthorhombic symmetry indicating a dominantly coaxial deformation (*pure shear* strain path). In the protomylonite (C12.2) the *c*-axis distribution is similar to the protolith

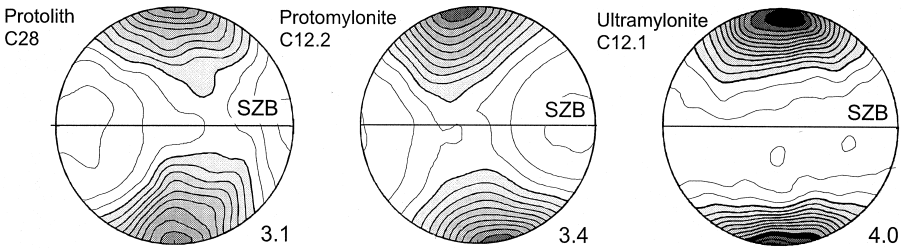


Fig. 4. Recalculated 0001 pole figures across the shear zone. Equal area, upper hemisphere projection normal to shear plane (SZB), lowest shaded contour equal to 1.0 × random, contour intervals 0.25 × random. The maximum pole density is given beside the diagrams.

but the maximum is slightly rotated with a sinistral sense of shear and the deviation of the girdle axis from x is to the opposite direction (Fig. 4). The texture of the ultramylonite exhibits a single *c*-axis maximum normal to the SZB (sample C12.1, Fig. 4). The maximum is highly symmetric and shows no tendency towards a girdle, contrary to C28 and C12.2.

## 3. Susceptibility measurements

For the AMS study, a total of 33 samples from the Thassos marble shear zone complex have been measured, 10 from the protolith, nine from the protomylonite and 14 from the ultramylonite. Measurements were undertaken in low fields (300 A/m, 920 Hz) using a Kappabridge KLY-2 (Geofyzika Brno, now AGICO). The sensitivity of this Kappabridge is given with $4 \times 10^{-8}$ (in SI-units) using a standard pick-up unit for 10 $cm^3$ nominal volume (KLY-2.1). We used standard AMS-cylinders, 2.5 cm in diameter and 0.82 × diameter in height, thus resulting in a sample volume of 10.8 $cm^3$. The directional susceptibility was determined for 15 positions with correction for the diamagnetic sample holder ($-1.3 \times 10^{-6}$). From this data the AMS tensor and the resulting magnitudes and orientation of the principal axes of the AMS-ellipsoids are calculated using the software package Ani20. In order to reduce measurement errors, the measurements have been repeated several times for each position until a stable value has been determined. To test the precision of the susceptibility values, we performed repeated measurements (12) for one position and found that the fluctuation of values within one position is significantly lower than the variation between two different measuring positions. Therefore we can state, that the determined anisotropies reflect the calcite texture and are not artificial.

In this study, $k_m$ expresses the volume susceptibility calculated as the mean value based on the magnitudes of the three principal ellipsoid axes ($k_{max}$, $k_{int}$, $k_{min}$). Shape ($T$) and degree of anisotropy ($P$) is displayed in Jelinek-diagrams where $T = 2 \ln (k_{int} - k_{min})/\ln (k_{max} - k_{min}) - 1$ which is >0 to +1 for oblate, 0 for neutral and <0 to −1 for prolate geometry (Jelinek, 1981). To express the anisotropy, we used the anisotropy degree $P$ ($k_{max}/k_{min}$). The geographic orientation of AMS-axes is presented in stereographic diagrams with projections into the lower hemisphere in equal area mode (Schmidt net). The mean value for the orientation of $k_{max}$, $k_{int}$ and $k_{min}$ and the $\alpha_{95}$ confidence angle, calculated by the program ASTA, are given as statistical parameters. The AMS data determined for the sample-set are compiled in Table 1. For more detailed descriptions of the AMS method see Hrouda (1982) or Tarling and Hrouda (1993).

### 3.1. Mean susceptibility and magnitudes of AMS

In all the samples mean susceptibility values are in the interval between $-11.5 \times 10^{-6}$ to $-13.9 \times 10^{-6}$, indicating only minor variations in mineralogical composition and verifying the diamagnetic behavior of the rocks. The single crystal susceptibility of $-12.87 \times 10^{-6}$ for calcite is given by Nye (1957). Therefore, the measured data are in coincidence with predicted susceptibilites for monomineralic calcite rocks. However, small differences in the mean values for the ultramylonites ($-12.73 \times 10^{-6}$) and the protolith ($-12.39 \times 10^{-6}$) and protomylonites ($-12.07 \times 10^{-6}$) were recorded.

Bestmann et al. (2000) observed optically minor amounts of dolomite in the mylonitic parts of the section. However, in X-ray diffraction it is lost in the background, and therefore a content of less than 2% has been estimated. Considering the single crystal data of dolomite ($-38 \times 10^{-6}$) reported in Borradaile et al. (1987), susceptibility will be expected to shift towards more negative values in the dolomite-bearing ultramylonites. A contribution of 1.5 vol.% dolomite would be enough to cause the difference in susceptibility recorded inside and outside the shear zones. Although such calculations are speculative, the shift towards more negative values excludes para- or ferrimagnetic contributions or Fe substitution in the calcite, which would cause shifts in the opposite direction.

For all the samples from the shear zones as well as from the protolith significant anisotropies have been determined (Fig. 5) with a slightly higher mean $P$ value of 1.040 for samples from the shear zones than from the protolith and protomylonites with 1.036 and 1.037. Distinct differences were recorded for the shape of the AMS-ellipsoids. In the protolith and protomylonite the shape factors generally

Table 1
Compilation of AMS parameters for the sample set

| Fabric type | Sample | $k$ | $k_{max}$ | $k_{int}$ | $k_{min}$ | $P$ | $T$ |
|---|---|---|---|---|---|---|---|
| Protolith | C31.2b | − 12.39 | 1.0173 | 0.9966 | 0.9861 | 1.031 | 0.224 |
| | C28.2b | − 12.97 | 1.1015 | 0.9977 | 0.9869 | 1.029 | − 0.236 |
| | C26.2.2b | − 11.87 | 1.0156 | 0.9985 | 0.9859 | 1.030 | − 0.143 |
| | C25b | − 13.02 | 1.0195 | 0.9975 | 0.9829 | 1.037 | − 0.192 |
| | C24.1.1 | − 12.14 | 1.0249 | 0.9999 | 0.9752 | 1.051 | 0.004 |
| | C12.4b | − 11.61 | 1.0175 | 0.9992 | 0.9833 | 1.035 | − 0.064 |
| | C12.3 | − 12.05 | 1.0235 | 0.9973 | 0.9792 | 1.045 | − 0.173 |
| | C17 | − 12.55 | 1.0216 | 0.9956 | 0.9828 | 1.039 | − 0.331 |
| | CI.14 | − 12.29 | 1.0134 | 0.9996 | 0.9870 | 1.027 | − 0.035 |
| | CI.8.1 | − 12.99 | 1.0178 | 0.9982 | 0.9841 | 1.034 | − 0.155 |
| | *Mean value* | *− 12.39* | *1.027* | *0.998* | *0.983* | *1.036* | *− 0.110* |
| | *STDV*[a] | *0.49* | *0.026* | *0.001* | *0.004* | *0.008* | *0.153* |
| Protomylonite | C22.2b | − 11.83 | 1.0194 | 0.9989 | 0.9817 | 1.038 | − 0.079 |
| | C19b | − 12.93 | 1.0160 | 1.0011 | 0.9829 | 1.034 | 0.108 |
| | C18 | − 12.59 | 1.0206 | 0.9990 | 0.9804 | 1.041 | − 0.066 |
| | C12.2b | − 12.10 | 1.0200 | 0.9971 | 0.9825 | 1.039 | − 0.221 |
| | C16.2b | − 12.77 | 1.0205 | 0.9965 | 0.9829 | 1.038 | − 0.267 |
| | C16.1b | − 11.77 | 1.0193 | 0.9961 | 0.9846 | 1.035 | − 0.328 |
| | C15.1z | − 11.47 | 1.0155 | 0.9972 | 0.9873 | 1.029 | − 0.289 |
| | C14.2b | − 11.57 | 1.0189 | 0.9992 | 0.9819 | 1.038 | − 0.059 |
| | C14.1b | − 11.62 | 1.0199 | 0.9994 | 0.9807 | 1.040 | − 0.037 |
| | *Mean value* | *− 12.07* | *1.019* | *0.998* | *0.983* | *1.037* | *− 0.138* |
| | *STDV*[a] | *0.55* | *0.002* | *0.002* | *0.002* | *0.004* | *0.145* |
| Ultramylonite | C32.2b | − 13.93 | 1.0285 | 0.9858 | 0.9857 | 1.043 | − 0.997 |
| | C35.2b | − 11.77 | 1.0253 | 0.9879 | 0.9868 | 1.039 | − 0.944 |
| | C12.1.2b | − 12.42 | 1.0310 | 0.9856 | 0.9834 | 1.048 | − 0.907 |
| | C11.b | − 12.42 | 1.0238 | 0.9910 | 0.9851 | 1.039 | − 0.691 |
| | C26.1.1b | − 12.88 | 1.0247 | 0.9898 | 0.9855 | 1.040 | − 0.810 |
| | C10.1.1 | − 12.80 | 1.0273 | 0.9888 | 0.9838 | 1.044 | − 0.765 |
| | C8.1.1b | − 12.80 | 1.0225 | 0.9915 | 0.9861 | 1.037 | − 0.700 |
| | C7.3.1b | − 13.01 | 1.0268 | 0.9889 | 0.9843 | 1.043 | − 0.777 |
| | C7.2.1b | − 13.27 | 1.0219 | 0.9902 | 0.9880 | 1.034 | − 0.867 |
| | C7.1.1b | − 13.37 | 1.0236 | 0.9903 | 0.9860 | 1.038 | − 0.767 |
| | C6.1 | − 12.32 | 1.0300 | 0.9860 | 0.9840 | 1.047 | − 0.914 |
| | C5.1 | − 13.01 | 1.0227 | 0.9907 | 0.9866 | 1.037 | − 0.770 |
| | C3.1.2b | − 12.65 | 1.0219 | 0.9900 | 0.9881 | 1.034 | − 0.891 |
| | C1.1.1 | − 11.51 | 1.0219 | 0.9914 | 0.9867 | 1.036 | − 0.729 |
| | *Mean value* | *− 12.73* | *1.025* | *0.989* | *0.986* | *1.040* | *− 0.824* |
| | *STDV*[a] | *0.63* | *0.003* | *0.002* | *0.001* | *0.004* | *0.096* |

[a] Standard deviation

indicate a triaxial symmetry with neutral to slightly prolate ellipsoids expressed by mean $T$-factors of $-0.11$ and $-0.14$. By contrast, the geometry within the shear zones is distinctly prolate with a mean value for the $T$-factors of $-0.82$. This sensitivity of the $T$-factor to the different calcite fabric types is also illustrated in Fig. 6, where the $T$-variation along the investigated section is shown. There is always a remarkable step in the shape of AMS recorded, when mylonitic parts of the section are entered. No systematic differences between protolith and protomylonite were encountered. Since AMS measurements integrate over the whole sample volume, small amounts of recrystallized grains in the protomylonites may be insignificant for the bulk fabric geometry.

### 3.2. Orientation of AMS-axes

The directions of the principal axes show a preferred orientation for all the fabric domains, with $k_{int}$ and $k_{min}$ oriented within and $k_{max}$ perpendicular to the SW-dipping foliation in both the protolith and mylonite (Fig. 7). This magnetic texture is in good agreement with the generally observed geometry of calcite textures with $c$-axes perpendicular to the mechanically active foliation (e.g. Schmid et al., 1981; Wenk et al., 1987; Ratschbacher et al., 1991; Erskine et al., 1993). However, there are significant differences in the geometry of the AMS-axis distributions inside and outside the shear zones that will be described below.

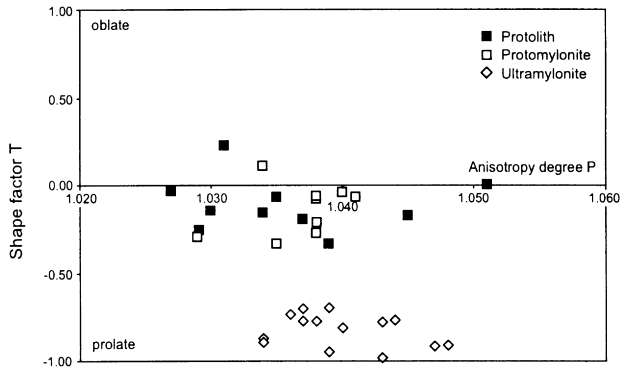


Fig. 5. *P–T* diagram for samples from the different fabric types. AMS-ellipsoids are neutral to slightly prolate in the protolith and protomylonite and strongly prolate in the ultramylonite.

In the protolith the $k_{max}$ axes generally have a perpendicular orientation to the macroscopically observed banding in the coarse marble (225/08), while the intermediate and minimum axes form clusters within this foliation. There is a weak tendency towards a girdle distribution around the $k_{min}$ direction. All the three axes of the AMS ellipsoids that are characterized by a triaxial geometry have clearly preferred orientations. The distribution of AMS axes in samples from the protomylonitic parts of the section resembles the protolith, however, while in the protolith $k_{min}$ forms a cluster. In the protomylonite $k_{min}$ tends to scatter within the plane of foliation or shear plane in the mylonitic parts, respectively. This holds also for the $k_{int}$ axes. In the ultramylonites, the direction of $k_{max}$ is well defined and forms a close cluster, while the $k_{int}$ and $k_{min}$ axes show a very wide scattering within the plane perpendicular to $k_{max}$.

For the interpretation of the magnetic fabric, it has to be taken into account that the single crystal anisotropy of calcite is uniaxial. The nearly perfectly prolate shapes of AMS ellipsoids determined for the ultramylonites (Figs. 5 and 6) are in very good agreement with the preferred orientation of *c*-axes in an axial symmetric distribution around the pole to the shear foliation (Fig. 4). For strongly prolate shapes the $k_{max}$ direction is well defined, while the intermediate and minimum axes have no preferred orientation within the plane perpendicular to $k_{max}$. The magnetic fabric for a single specimen is perfectly prolate and the overall magnetic fabric for the whole ultramylonitic sample set has the same symmetry. However, the anisotropy is reduced from 1.113 for a single crystal to 1.04 for the magnetic fabric in the ultramylonites. This reduction can be explained by envisaging a calcite single crystal with a *c*-axis axis perpendicular to the shear plane (Fig. 8). Small deviations from this perpendicular orientation give rise to an axial-symmetrical distribution pattern, which leads to a reduction in the bulk magnetic anisotropy.

In the protolith and protomylonite the magnetic fabric of the individual specimens are triaxial (neutral to slightly prolate shapes, Figs. 5 and 6) and the overall geometry for both the sample sets is orthorhombic. This geometry reflects

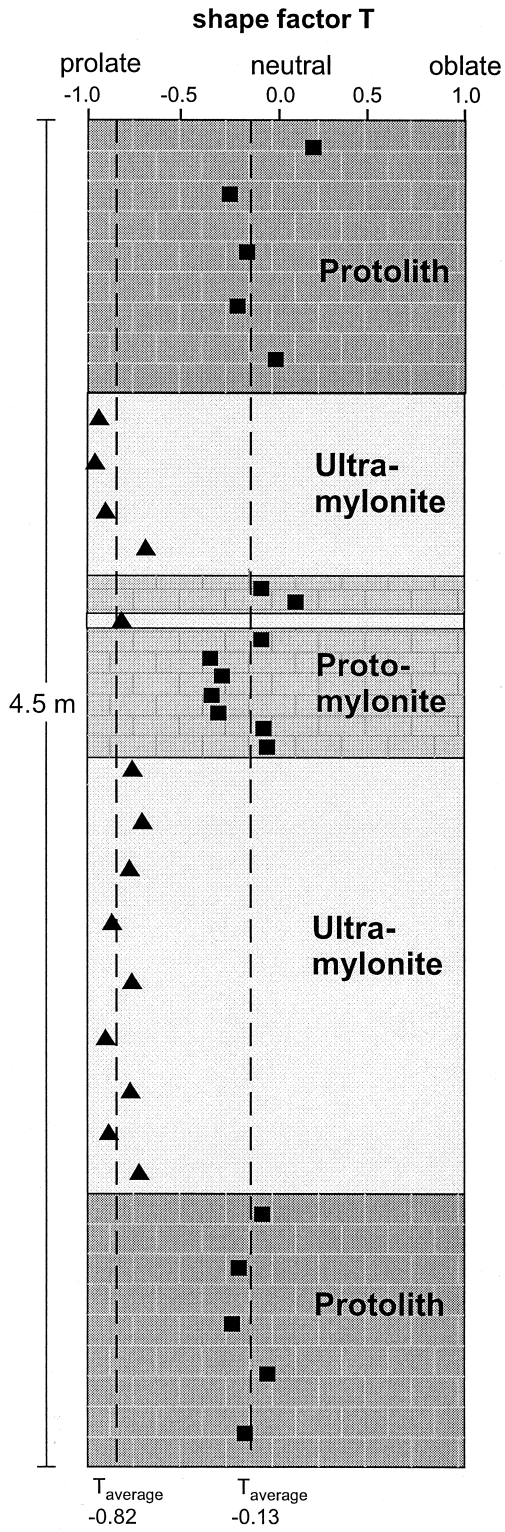


Fig. 6. Variation of the shape factor *T* in the marble shear zone complex.

very well the girdle tendency of *c*-axes around the *X*-direction (direction of shear in the mylonites) that has been determined by texture analyses (Fig. 4). The rotation of prolate calcite single crystals around a lineation will reduce the magnitude of susceptibility in the $k_{max}$ direction

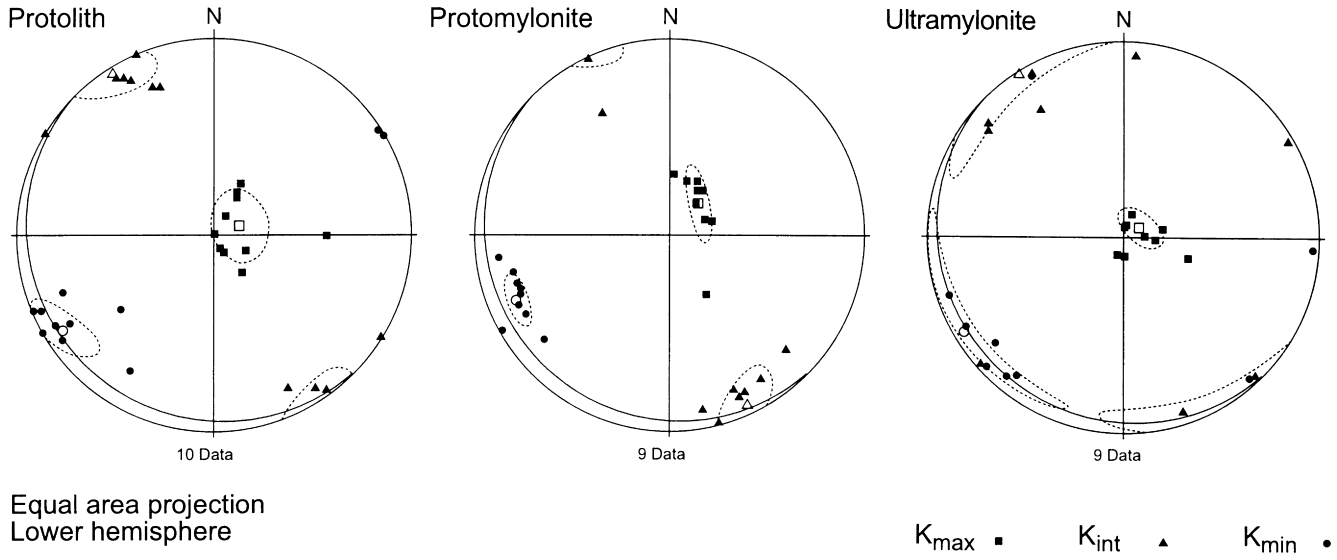


Fig. 7. AMS principal axes for the three fabric types in geographic orientation. Mean orientation with $\alpha_{95}$ confidence angles for $k_{max}$, $k_{int}$ and $k_{min}$ are given for each sample set. All main tectonic planes in both protolith and shear zones are observed to be subparallel with a mean orientation of 225/08 (dip-direction/dip) (see Fig. 2) which is shown as great circle.

at the expense of the $k_{int}$ direction while the magnitude for $k_{min}$ remains the same (Fig. 8). If the rotation is large enough it will induce a triaxial (neutral) shape for the bulk anisotropy.

## 4. Recalculation of AMS from calcite textures

The prediction of the AMS of a polycrystal is based on the texture and single crystal anisotropy of the considered minerals. It is assumed that the overall AMS is an algebraic mean over all crystals in a sufficiently large sample volume, weighted with the orientation density related to the actual orientation (refer to Tomé, 1998, for the fundamentals). However, the AMS is not constant for the single crystal due to the occurrence of grain boundaries, which represent discontinuities. These discontinuities can be considered in a different way, as demonstrated by Bunge (1985) for the elastic tensor. The Voigt averaging technique assumes no discontinuities in the direction of an applied uniaxial stress, i.e. the strain is homogeneous within the sample and the calculated value gives the upper limit for elastic deformation. The Reuss approximation is based on the arrangement of discontinuities perpendicular to the direction of applied stress, i.e. the stress is homogeneous within the sample and the elastic strain is a minimum. It has been demonstrated by Hill (1967) that the mean between the two values is more probable. Although questionable, the Voigt and Reuss models have been applied to second rank tensors as well. We used them both for our calculations to obtain an interval, which should contain the measured AMS. As single crystal anisotropy $P = k_{max}/k_{min}$ we used the value of $P = 1.113$ reported by Owens and Bamford (1976), which is based on measurements from Nye (1957). Due to the axial symmetry of the single crystal AMS with the *c*-axis as the symmetry axis, the AMS may be modeled from the 0001 pole figure only. In practice, the ODF was represented by means of C-coefficients (Dahms and Bunge, 1989) and the AMS was calculated from the C-coefficients. For the fundamentals on the estimation of tensorial properties from C-coefficients refer to Siegesmund (1996).

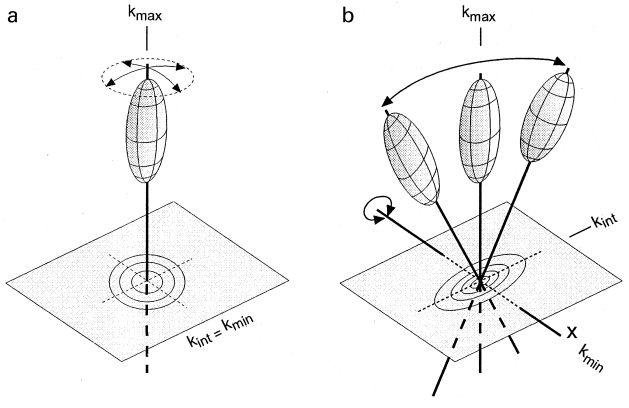


Fig. 8. Sketch to demonstrate the relationship between uniaxial single crystal ellipsoids and the observed magnetic fabric symmetry (a) in the ultramylonite and (b) in the protolith and protomylonite. (a) Small deviations of the *c*-axis from a perpendicular orientation to the shear plane give rise to an axial-symmetrical distribution pattern will reduce the bulk magnetic anisotropy compared to the anisotropy of the single crystal. (b) Neutral (triaxial) AMS-fabrics as observed in the protolith and protomylonite can develop by the rotation of uniaxial ellipsoids around a linear element.

Examples for the calculated susceptibility distribution are presented as contour diagrams (Fig. 9). The plots are given with respect to the reference system introduced in section 1.1, which has been also used for the presentation of the pole figures in Fig. 4. From the recalculated susceptibility tensors for the Voigt and Reuss approximation the factors

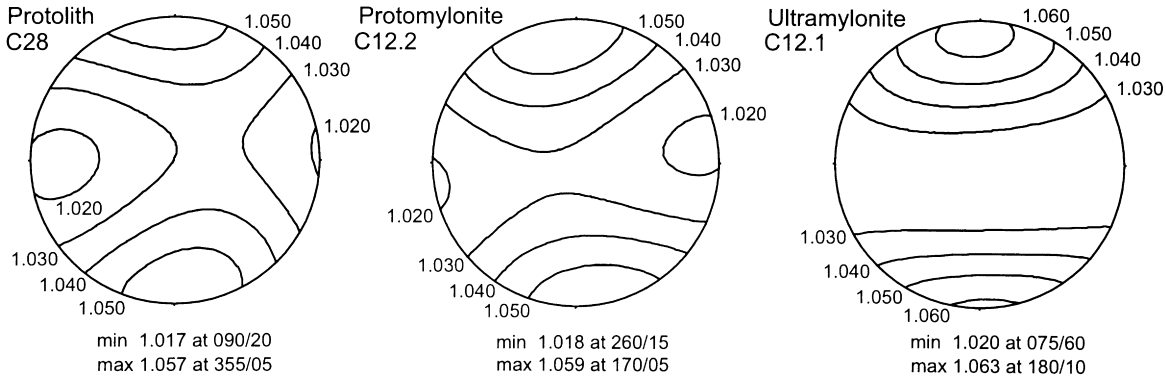


Fig. 9. Calculated susceptibility distribution on the base of the orientation distribution function (ODF) for calcite. Reference system as in Fig. 4. Projection into the upper hemisphere.

describing the shape ($T$) and degree of anisotropy ($P$) of the AMS-ellipsoids were calculated. These factors and the orientations of the principal axes of the recalculated AMS-ellipsoids are compiled in Table 2.

The Jelinek diagram in Fig. 10 presents the shape factor ($T$) and the anisotropy degree ($P$) of the recalculated AMS considering the single crystal anisotropy of $P = 1.113$. Shape and anisotropy reflect the general change of triaxial to uniaxial ellipsoids accompanied by an increase in the anisotropy $P$ during progressive deformation from protolith to protomylonite and ultramylonite. For all the three samples the recalculated data show generally lower $P$ values for the Voigt approximation than for the Reuss model. These differences are significantly higher for C28 (protolith) and C12.2 (protomylonite) than recorded in C12.1 (ultramylonite). For C28 and C12.2 the ellipsoid shape is slightly more prolate for the Reuss than for the Voigt model with $-0.191$ compared to $-0.133$ in the protolith and $-0.357$ compared to $-0.293$ in the protomylonite. For the ultramylonite the situation is vice versa with $-0.763$ and $-0.768$, respectively (Table 2).

### 4.1. Comparison of modeled and measured AMS

The orientations of the principal axes of measured and recalculated AMS ellipsoids are compared in Fig. 11. For the protolith there is a strong parallelism between the orientations of modeled and measured axes, which holds for all the three axes. Due to the triaxial symmetry of the AMS-ellipsoid for this sample, with a shape factor of $T = 0.173$, there are significant differences in the magnitudes of susceptibility for all the three axes. Thus, the positions of all three axes are well defined.

In the protomylonite and in the ultramylonite, it is seen that the $k_{max}$ directions show high coincidence in orientation, while the $k_{int}$ and $k_{min}$ axes deviate. In the protomylonite, this deviation is less pronounced than in the ultramylonite. This is in good agreement with the change from a distinctly prolate to a perfectly prolate shape of the AMS when proceeding from protomylonite to ultramylonite. This change in shape will reduce the differences in the magnitudes between $k_{int}$ and $k_{min}$ and correspondingly reduce the precision with which the axis directions are defined (see Fig. 11).

In Fig. 12 the recalculated anisotropy and shape factors are compared with the measured AMS data. For the recalculated data, the mean between Voigt and Reuss approximation values (Hill, 1967) is presented. For both the data sets a trend from triaxial to uniaxial ellipsoids is related to an increase in the degree of anisotropy.

## 5. Discussion

In general, the magnetic fabric in both the protolith and

Table 2
Recalculated (Reuss and Voigt model) and measured (AMS) magnetic fabric parameters.

| | C28 (Protolith) | | | C12.2 (Protomylonite) | | | C12.1 (Ultramylonite) | | |
|---|---|---|---|---|---|---|---|---|---|
| | Reuss | Voigt | AMS | Reuss | Voigt | AMS | Reuss | Voigt | AMS |
| L | 1.023 | 1.023 | 1.016 | 1.027 | 1.027 | 1.032 | 1.037 | 1.038 | 1.046 |
| F | 1.016 | 1.018 | 1.022 | 1.013 | 1.015 | 1.009 | 1.005 | 1.005 | 1.002 |
| P | 1.039 | 1.041 | 1.039 | 1.040 | 1.042 | 1.041 | 1.042 | 1.043 | 1.048 |
| T | − 0.191 | − 0.133 | 0.173 | − 0.357 | − 0.293 | − 0.559 | − 0.763 | − 0.768 | − 0.909 |
| $k_{max}$ | 355/05 | | 178/04 | 170/05 | | 172/03 | 180/10 | | 173/11 |
| $k_{int}$ | 252/69 | | 283/74 | 062/74 | | 078/52 | 085/30 | | 359/79 |
| $k_{min}$ | 090/20 | | 087/16 | 260/15 | | 264/38 | 295/60 | | 263/01 |

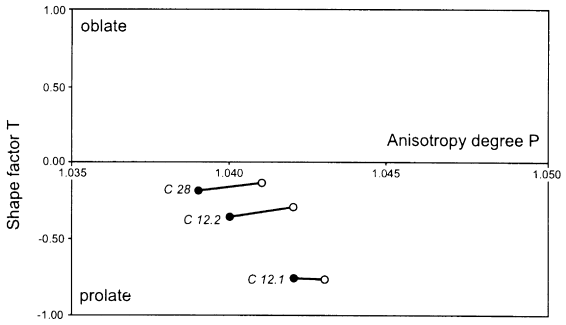


Fig. 10. Recalculated shape and anisotropy for the 3 samples C28 (protolith), (C12.2) (protomylonite) and C12.1(ultramylonite) based on a single crystal anisotropy of 1.113. Filled dots give the values for Voigt, unfilled for Reuss approximation.

the protomylonite is in agreement with the pure shear deformation geometry that Bestmann et al. (2000) interpreted from microstructural observations and texture analyses. We found the maximum susceptibility, which in a single crystal is in the direction of the *c*-axis, to be in an orientation perpendicular to the macroscopic foliation in the protolith and perpendicular to shear foliation in the protomylonite, respectively. Deformation in a pure shear regime will cause an orthorhombic symmetry with preferred orientations of *c*-axes parallel to, and orientation of *a*-axis normal to the direction of compression, respectively (Wenk, 1985; Wenk et al., 1987).

The fabric in the ultramylonites is described by Bestmann et al. (2000) as a *steady state* microstructure where the preferred crystallographic orientation is the result of the activity of slip systems with a stable end orientation of *easy slip*. The magnetic fabric reflects this microstructure by the highly symmetrical cluster of $k_{max}$ resulting in nearly perfectly prolate shapes oriented perpendicular to the shear planes.

So far, there are few studies on quantitative relations between AMS and preferred orientation of minerals. Recalculation of AMS from textures has been performed by Siegesmund et al. (1995) who investigated the quantitative relationship between mica-preferred orientation and magnetic fabric (low-field AMS) for different rock types (orthogneisses, granulites, mylonites). They found very variable degrees of coincidence between both these fabrics. Similar results were reported for mica-bearing rock types by Hrouda et al. (1997) who did recalculations based on the calculation of the theoretical AMS from the principal values of the orientation tensor for the phyllosilicate fabric (Hrouda and Schulmann, 1990).

All these investigations in polymineralic rocks suffer the general problems that subfabrics of the individual mineralogical components can interfere. In addition only small amounts of ferrimagnetic minerals can have strong influences on the recalculations. Therefore, it is evident that monomineralic rocks are more suitable for such modelling. Hrouda (1980) investigated the quantitative relation between texture and magnetocrystalline anisotropy of the magnetically uniaxial minerals pyrrhotite and hematite and found good correlations in cases where the *c*-axes show a distinct preferred orientation.

For the monomineralic Thassos marble there is an excellent correlation for the direction of the principal axes of AMS-ellipsoids between measured and modeled data sets. The measured shapes follow a trend from neutral towards perfectly prolate as has also been modeled from texture data (Fig. 12). A high sensitivity of the shape factor *T* relative to strain has also been found in a quantitative deformation analysis of upper greenschist facies metabasites using combined AMS and optical fabric investigations (Schobel and de Wall, 1999). This study demonstrates that increments of a progressive deformation path can be very well reflected by changes in the shape of AMS-ellipsoids.

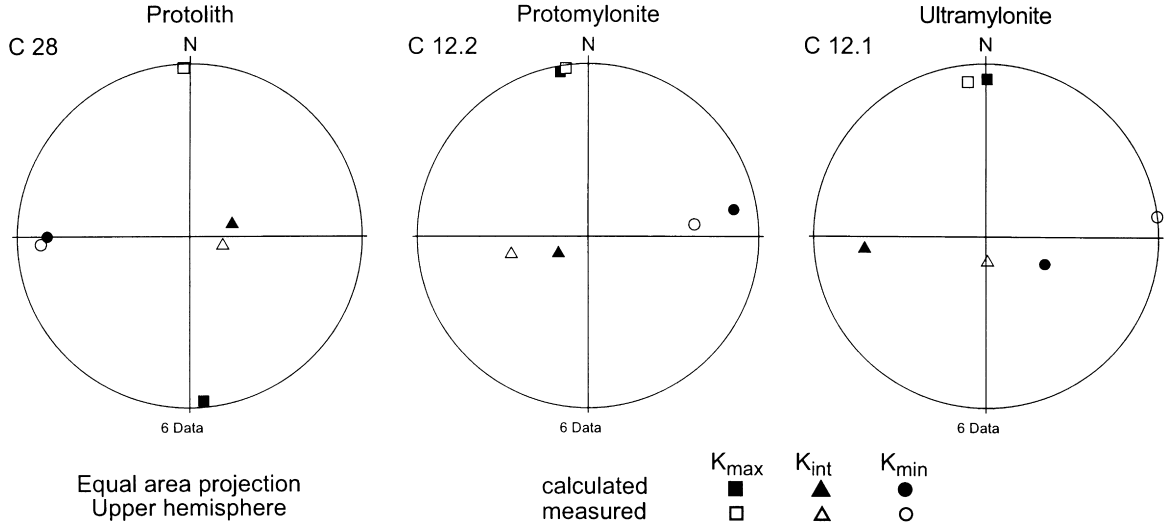


Fig. 11. Comparison of measured and calculated AMS-axes for protolith, protomylonite and ultramylonite. The reference system, E–W direction = x, *N* = pole to the shear zone boundary, is the same as in Figs. 4 and 9.

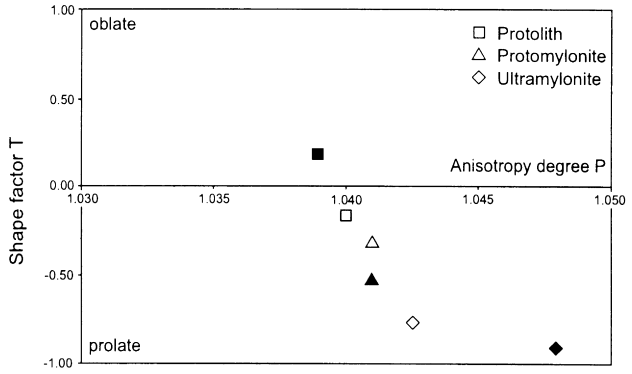


Fig. 12. Comparison of measured (black symbols) and modeled (grey symbols) magnetic anisotropy data in a $P$–$T$ diagram. For the modelled data the mean between Voigt and Reuss approximation (compare Fig. 10) is presented according to Hill (1967).

Recalculated anisotropy values of about 4% are in good agreement with the measured data. However, in the ultramylonitic sample differences do occur between the measured (1.048) and modeled (1.043) degree of anisotropy (Fig. 12). This might indicate that the single crystal anisotropy of 1.113 taken for the recalculations is valid only for the coarse-grained, twinned protolith and protomylonitic fabric, but does not reflect the anisotropy of the fine-grained, recrystallized fabric of the ultramylonite. A significantly higher single crystal anisotropy (from our calculation: $P = 1.13$) would be needed to achieve the measured value. On the other hand it has to be taken into account that variations in susceptibility of $4 \times 10^{-8}$, which is the sensitivity limit for the KLY-2 Kappabridge, will produce differences in $P$ of 0.003 in the investigated calcites. Therefore it cannot be excluded that the observed difference between measured and modeled anisotropy is partly caused by errors in measurement of the AMS.

An additional point of discussion concerns the larger difference in recalculated anisotropy between Voigt and Reuss approximations in the protolith and protomylonite magnetic fabrics, as compared to the ultramylonite (Fig. 10). It can be speculated that this reflects the varying microstructural states of the calcite fabric, such as grain size variations, grain boundary orientation and twin-lamellae density (Fig. 3). Theoretically this can be inferred from the model applied and has been reported for recalculations of elastic properties in copper (Bunge, 1985). However, to test the significance of variations in single crystal anisotropy or twin-density and twin-orientation for the recalculations, better constrains from experimental data are needed.

## 6. Conclusions

Our study has shown that the low field AMS-technique is applicable also to diamagnetic rocks if the equipment is sensitive enough to record differences in the magnitude of susceptibility in the order of $10^{-7}$ to $10^{-8}$ SI units. The marble complex of Thassos Island consists of calcite with minor contributions of quartz and dolomite and is free of any paramagnetic or ferromagnetic constituents. The low-field susceptibility shows pure diamagnetic behaviour consistent with values reported for single calcite crystals. Mineralogical differences between protolith and ultramylonites may be documented by differences in the mean respective susceptibility. Progressive shear deformation transforms AMS ellipsoids from triaxial (neutral) to uniaxial (prolate) shapes.

The recalculation from mineral textures for such a monomineralic rock type shows a very good coincidence in the orientation of principal axes between measured and modeled AMS. A modification in shape of the recalculated AMS from neutral to distinct prolate ellipsoids with generally increasing anisotropy degree ($P$) is consistent with the measured magnetic fabric evolution with progressive deformation.

## Acknowledgements

Many thanks to L. Nano for help in preparing the figures and to F. Schobel for assistance in the laboratory. We are particularly grateful to B. Housen and W.H. Owens for their constructive reviews and to R.O. Greiling and L.N. Warr for valuable feedback. Michel Bestmann kindly acknowledges the financial support of the Graduiertenförderung (Bayern) and Klaus Ullemeyer support through BMBF grant 03-DUBGO2.

## References

Adams, B.L., Dingley, D.J., Kunze, K., Wright, S.I., 1994. Orientation imaging microscopy: new possibilities for microstructural investigations using automated BKD analysis. In: Bunge, H.J. (Ed.), Textures of materials, ICOTOM 10. Materials Science Forum 157-162, pp. 31–42.

Bestmann, M. Kunze, K. Matthews, A., 2000. Evolution of a calcite marble shear zone complex on Thassos Island, Greece: Microstructural and textural fabrics and their kinematic significance. Journal of Structural Geology 22, 1789–1807.

Borradaile, G., 1987. Anisotropy of magnetic susceptibility: rock composition versus strain. Tectonophysics 138, 327–329.

Borradaile, G.J., Keeler, W., Alford, C., Sarvas, P., 1987. Anisotropy of magnetic susceptibility of some metamorphic minerals. Physics of the Earth and Planetary Interiors 48, 161–166.

Dahms, M., Bunge, H.J., 1989. The iterative series-expansion method for quantitative texture analysis—General Outline. Journal of Applied Crystallography 22, 439–447.

Erskine, B.G., Heidelbach, F., Wenk, H.-R., 1993. Lattice preferred orientation and microstructures of deformed Cordilleran marbles: correlation of shear indicators and determination of strain path. Journal of Structural Geology 15, 1189–1205.

Hill, R., 1967. The essential structure of constitutive laws for metal composites and polycrystals. Journal of Mechanics and Physics of Solids 15, 79–95.

Hrouda, F., 1980. Magnetocrystalline anisotropy of rocks and massive ores: a mathematical model study and its fabric implications. Journal of Structural Geology 2, 459–462.

Hrouda, F., 1982. Magnetic anisotropy of rocks and its application in Geology and Geophysics. Geophysical Surveys 5, 37–82.

Hrouda, F., 1986. The effect of quartz on the magnetic anisotropy of quartzite. Studia Geophysica Geogyn 30, 39–45.

Hrouda, F., Schulmann, K., 1990. Conversion of the magnetic susceptibility tensor into the orientation tensor in some rocks. Physics of the Earth and Planetary Interiors 63, 71–77.

Hrouda, F., Schulmann, K., Suppes, M., Ullemeyer, K., de Wall, H., Weber, K., 1997. Quantitative Relationship between Low-Field AMS and Phyllosilicate Fabric: A Review. Physics and Chemistry of the Earth 22, 153–156.

Kunze, K., Heidelbach, F., Wenk, H.-R., Adams, B.L., 1994. Orientation Imaging Microscopy of Calcite Rocks. In: Bunge, H.J., Siegesmund, S., Skrotzki, W., Weber, K. (Eds.), Textures of Geological Materials. DGM Informationsgesellschaft, Oberursel, pp. 279–302.

Jelinek, V., 1981. Characterization of the magnetic fabric of rocks. Tectonophysics 79, 63–67.

Matthies, S., Vinel, G.W., 1982. On the reproduction of the orientation distribution function of textured samples from reduced pole figures using the conception of a conditional ghost correction. Physical Status Solidi (b) 112, K111–K120.

Nye, J.F., 1957. Physical Properties of Crystals. Oxford University Press, Oxford.

Owens, W.H., Bamford, D., 1976. Magnetic, seismic and other anisotropic properties of rock fabrics. Philosophical Transactions of the Royal Society of London A283, 55–68.

Owens, W.H., Rutter, E.H., 1978. The development of magnetic susceptibility anisotropy through crystallografic preferred orientation in a calcite rock. Physics of the Earth and Planetary Interiors 16, 215–222.

Peterek, A., Polte, M., Wölfl, C., Bestmann, M., Lemtis, O., 1994. Zur jungtertiären geologischen Entwicklung im SW der Insel Thassos (S-Rhodope, Nordgriechenland). Erlanger geologische Abhandlungen 124, 29–59.

Ratschbacher, L., Wenk, H.-R., Sintubin, M., 1991. Calcite textures: examples from nappes with strain-path partitioning. Journal of Structural Geology 13, 369–384.

Rutter, E., Rusbridge, M., 1977. The effect of non-coaxial strain paths on crystallographic preferred orientation development in the experimental deformation of a marble. Tectonophysics 88, 201–233.

Schmid, S.M., Casey, M., Starkey, J., 1981. The microfabric of calcite tectonites from the Helvetic nappes (Swiss Alps). In: McClay, K.R., Price, N.J. (Eds.). Thrust and Nappe Tectonics. Special Publications of the Geological Society of London 9, pp. 151–158.

Schobel F., de Wall, H., 1999. Quantitative deformation analysis of upper greenschist facies metabasites using combined AMS and optical fabric investigations. International Conference on Textures and Physical Properties of Rocks, 13-16.Oct., Göttingen, Abstract Volume. Göttinger Arbeiten zur Geologie und Paläontologie Sb4, 33-34.

Siegesmund, S., 1996. The significance of rock fabrics for the geological interpretation of geophysical anisotropies. Geotektonische Forschungen 85, 1–123.

Siegesmund, S., Ullemeyer, K., Dahms, M., 1995. Control of rock magnetic fabrics by mica preferred orientation: a quantitative approach. Journal of Structural Geology 17, 1601–1613.

Tarling, D.H., Hrouda, F., 1993. The Magnetic Anisotropy of Rocks. Chapman and Hall, London.

Tomé, C.N., 1998. Tensor properties of textured polycrystals. In: Kocks, U.F., Tomé, C.N., Wenk, H.-R. (Eds.), Texture and Anisotropy, Cambridge University Press, Cambridge, pp. 282–325.

Ullemeyer, K., Spalthoff, P., Heinitz, J., Isakov, N.N., Nikitin, A.N., Weber, K., 1998. The SKAT texture diffractometer at the pulsed reactor IBR-2 at Dubna: experimental layout and first measurements. Nuclear Instruments and Methods in Physics Research A412, 80–88.

Van Daalen, M., Heilbronner, R., Kunze, K., 1999. Orientation analysis of localized shear deformation in quartz fibres at the brittle-ductile transition. Tectonophysics 303, 83–107.

Wawrzenitz, N., Krohe, A., 1998. Exhumation and doming of the Thassos metamorphic core complex (S Rhodope, Greece): structural and geochronological constraints. Tectonophysics 285, 301–332.

Wenk, H.-R., 1985. Carbonates. In: Wenk, H.-R. (Ed.), Preferred Orientation in Deformed Metals and Rocks: An Introduction to Modern Texture Analysis. Academic Press, Orlando, pp. 361–384.

Wenk, H.-R., Takeshita, T., Bechler, E., Erskine, B.G., Matthies, S., 1987. Pure shear and simple shear calcite textures. Comparison of experimental, theoretical and natural data. Journal of Structural Geology 9, 731–745.

Wenk, H.R., Matthies, S., Donovan, J., Chateigner, D., 1998. BEARTEX: A windows-based program system for quantitative texture analysis. Journal of Applied Crystallography 31, 262–269.